Biophysical Chemistry 189 (2014) 40–48

Contents lists available at ScienceDirect

Biophysical Chemistry

journal homepage: http://www.elsevier.com/locate/biophyschem

Synchrotron based infrared imaging and spectroscopy via focal plane array on live fibroblasts in D_2O enriched medium

Luca Quaroni [a,*], Theodora Zlateva [a], Blagoj Sarafimov [a], Helen W. Kreuzer [b], Katia Wehbe [c], Eric L. Hegg [d], Gianfelice Cinque [c]

[a] Paul Scherrer Institut, Villigen-PSI, CH-5232, Switzerland
[b] Pacific Northwest National Laboratory, Richland, WA 99354, USA
[c] Diamond Light Source, Harwell Campus, Chilton–Didcot, Oxon OX11 0DE, UK
[d] Michigan State University, Department of Biochemistry & Molecular Biology, East Lansing, MI 48824, USA

HIGHLIGHTS

- We use synchrotron infrared imaging to study biochemical and biophysical processes in living cells.
- We can observe distribution and conformational properties of lipids.
- We can measure the kinetics of hydrogen/deuterium exchange in cellular locations.
- We can image gradients of isotopic concentration associated to metabolism.

GRAPHICAL ABSTRACT

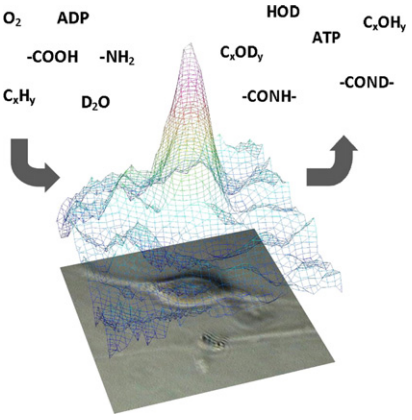

ARTICLE INFO

Article history:
Received 3 February 2014
Received in revised form 15 March 2014
Accepted 16 March 2014
Available online 26 March 2014

Keywords:
Infrared spectromicroscopy
Synchrotron radiation
Single cell
Cell lipid
Isotope tracer
Full-field IR microscopy

ABSTRACT

We successfully tested the viability of using synchrotron-based full-field infrared imaging to study biochemical processes inside living cells. As a model system, we studied fibroblast cells exposed to a medium highly enriched with D_2O. We could show that the experimental technique allows us to reproduce at the cellular level measurements that are normally performed on purified biological molecules. We can obtain information about lipid conformation and distribution, kinetics of hydrogen/deuterium exchange, and the formation of concentration gradients of H and O isotopes in water that are associated with cell metabolism. The implementation of the full field technique in a sequential imaging format gives a description of cellular biochemistry and biophysics that contains both spatial and temporal information.

1. Introduction

Infrared (IR) absorption spectroscopy is a valuable technique for the identification and characterization of molecular substances and their

* Corresponding author at: University of Fribourg, Department of Chemistry, Fribourg, CH-1700, Switzerland. Tel.: +41 62 8711130.
E-mail address: quaroni@bluewin.ch (L. Quaroni).

http://dx.doi.org/10.1016/j.bpc.2014.03.002

dynamics. The coupling of Fourier transform infrared (FTIR) technology for spectral analysis and of infrared microscopes for beam focusing and accurate sample location has generated a rapid growth of spectromicroscopy and imaging applications [1].

One current direction of development is the use of FTIR spectromicroscopy ex vivo for the study of processes in functional cells with single cell resolution [2,3]. Frequently this requires immersion in an aqueous medium, particularly when working with eukaryotic cell lines. Transmission measurements in an aqueous environment are constrained by the strong IR absorption of water, and consequent decreased light throughput, often covering spectral features of interest. The problem can be reduced in a micro-ATR imaging experiment [4], but this configuration is not always accessible and has some limitations. In addition, measurements on non-fixed samples are complicated by the nature of the living cell itself, which can move through the medium either because of free flotation or because of cellular motility, thus requiring rapid measurements. All these challenges combine with the ones already associated to FTIR measurements of single cells, namely the simultaneous need for high spatial resolution, high signal-to-noise (S/N) ratio and good spectral resolution. It has been shown that the use of IR microscopes in a confocal configuration, particularly when coupled to synchrotron radiation (SR), allows time resolved spectromicroscopy measurements in an aqueous environment with single cell or subcellular resolution in less than one minute [5]. However, measurement of the two-dimensional distribution of infrared spectra throughout a living individual cell is often performed using a raster scanning approach with SR light, particularly when diffraction limited spatial resolution is required together with high quality absorption spectra. In recent years, focal plane array (FPA) detectors have greatly expanded the capability of infrared microscopes to collect rapidly large two-dimensional sets of spectra [1]. In a recent review on the coupling of FPA detectors to SR [6], the notion of improved data quality is introduced both in terms of S/N advantage and optimization of sample size imaged per pixel. The coupling of FPA-fitted microscopes with synchrotron sources is now promising to allow even faster rates of spectral collection at high S/N ratios [7–9].

In this work we describe the first use of a SR light source and FPA microscope for the rapid transmission imaging of a living cell. We show that the setup at the MIRIAM beamline at Diamond Light Source allows the collection of high resolution IR images of single viable cells in a few minutes. The S/N ratio for the spectra is of such quality as to allow resolution and mapping of the individual spectral components in the overlapping bands of C–H bonds stretching modes. We also show that the maps allow us to study both steady-state processes, such as concentration gradients in the proximity of the cell, and dynamic ones, such as hydrogen–deuterium exchange (H/D) at selected cellular locations.

2. Experimental

2.1. Fibroblast cell culture for FTIR spectromicroscopy measurements

The Cell Culture Laboratory of beamline B22 at Diamond Light Source was used for cell culture procedures. NIH 3T3 Swiss albino mouse fibroblast cells (ECACC catalog number 85022108) were cultured directly on CaF_2 windows (Crystran, Poole, UK) in Dulbecco's Modified Eagle Medium (DMEM), with high glucose concentration and supplemented with 10% fetal bovine serum. The cells were grown for 16 to 24 h, until the desired degree of confluency was obtained (about 20%–30%). All the cell culture materials were purchased from Invitrogen (Invitrogen, Life Technologies, Paisley, UK) [10].

2.2. Fibroblast cell treatment

Just before the FTIR measurement, the cell-coated window was rinsed with serum-free DMEM. This was followed by three washes with DMEM prepared in D_2O (99% final concentration). The washing was performed by removing the slide from the culture dish, draining the old medium and adding 200 μl of D_2O-enriched medium to the top of the window [10]. The operation was repeated three times. The cell covered window was then inserted into a custom-built solution sample holder for FTIR microscopy, as previously described [2,10]. The sample holder was topped-off with D_2O-enriched medium, closed, kept at room temperature, and used for FTIR spectromicroscopy measurements. About 2 to 4 min elapsed between the exposure of cells to D_2O-enriched medium and the first measurement.

2.3. FTIR imaging measurements

Experiments were performed at the MIRIAM beamline (B22) of Diamond Light Source, comprising a Bruker Vertex 80v interferometer (Bruker Optics, Ettlingen, Germany) and a Bruker Hyperion 3000 microscope. A summary of MIRIAM parameters and mid-IR performances for diffraction-limited FTIR microanalysis is in reference [11]. An original triple mirror system was used both to couple the large horizontal SR fan to the interferometer entrance so to operate a longitudinal compression of the geometrical source [12], i.e. to exploit the SRIR high-brightness.

SR FTIR images were acquired with the downstream microscope by means of the liquid nitrogen-cooled FPA photovoltaic MCT detector 64 × 64 pixels in transmission mode, using a 36× objective. Homogeneous illumination of the sample area was achieved via the 15× condenser. The field of view accessible by the FPA was circa 70 × 70 μm^2, i.e. covering the cell body and the long fibroblast "tails" in a single snapshot. The 40 × 40 μm^2 single pixel area at the FPA detector is demagnified by a factor of 36×, to an effective area of 1.1 × 1.1 μm^2 at the sample position. It must be emphasized that pixel size is different from resolution, being smaller than the spatial resolution, as denoted by the Rayleigh criterion for diffraction limited resolution. Nonetheless this image oversampling is a prerequisite to utilize all IR absorption information passed by the sample into the FTIR spectroscopic image, as detailed in the discussion.

For these measurements, a KBr-supported Ge-multilayer beamsplitter allowing the full mid-IR range was used. Measurements were performed in transmission mode. For each measurement 256 scans were collected at 4 cm^{-1} resolution, with a 20 min interval between measurements. Single channel spectra were obtained by performing a Fourier transform of the interferogram after apodization with a Blackman–Harris 3-term function, using a zero-filling factor of 2 and a power phase correction.

The FTIR maps obtained with OPUS were matched to the visible image of the cell by correcting for the offset between the visible and IR field of view, corresponding to a vertical translation of about 5 μm. Overlayed visible and IR images were then used to represent the spatial distribution of absorption bands. IR maps were plotted using the 2nd derivative of absorption spectra, calculated with Savitzky–Golay 9-point smoothing. The scale of individual IR maps was adjusted to exclude background absorption from the map.

3. Results

3T3 NIH fibroblast cells were grown on CaF_2 slides in complete DMEM medium and gently washed with DMEM prepared in 99% D_2O just prior to IR imaging measurements. The CaF_2 window covered with D_2O DMEM-rinsed cells was then enclosed in a sample holder for liquid media, and 2D infrared images were collected at 20 minute intervals at the downstream endstation of MIRIAM beamline B22 of Diamond. We have previously shown that exposure to such high concentrations of D_2O, although stressful for the cells [13], does not compromise their viability. The use of Trypan Blue in parallel tests confirms that under these conditions the cellular membrane remains intact throughout the duration of the measurements [10].

3.1. High spatial and spectral resolution imaging of C–H vibrations

Fig. 1A shows the visible light image of a fibroblast cell collected with the video camera of the Bruker IR microscope. Fig. 1B shows the absorption spectrum around the C–H stretching region recorded from one cellular location and Fig. 1C shows the corresponding second derivative. The extended spectrum covering the full mid IR region is shown in Figure S1 of the Supplementary Information. Fig. 1D and E shows IR images obtained by mapping the distribution in space of specific absorption bands.

To reduce the relative spectral contribution of optical effects different from light absorption, maps have been calculated by plotting the intensity of the second derivative of the spectrum [14]. A complication of this approach is the reduced signal-to-noise ratio in derivative spectra when compared to the original absorption spectra. Nonetheless, in our measurements the S/N ratio in the absorbance spectra is sufficiently high that, even after derivation, high quality maps can still be obtained.

An additional advantage of the use of second derivatives is the possibility to increase spectral resolution by taking advantage of the sharper central peak in the second derivative. To stress the gain in spectral resolution, Fig. 1B highlights the multiplet observed in the 2800–3000 cm^{-1} spectral region. This is typically assigned to stretching modes of the $CH/CH_2/CH_3$ groups. In samples containing long chain alkyl or acyl groups, this multiplet is dominated by strong absorption bands from the symmetric and antisymmetric stretching modes of CH_2 units around 2855 and 2923 cm^{-1}. Weaker contributions from a

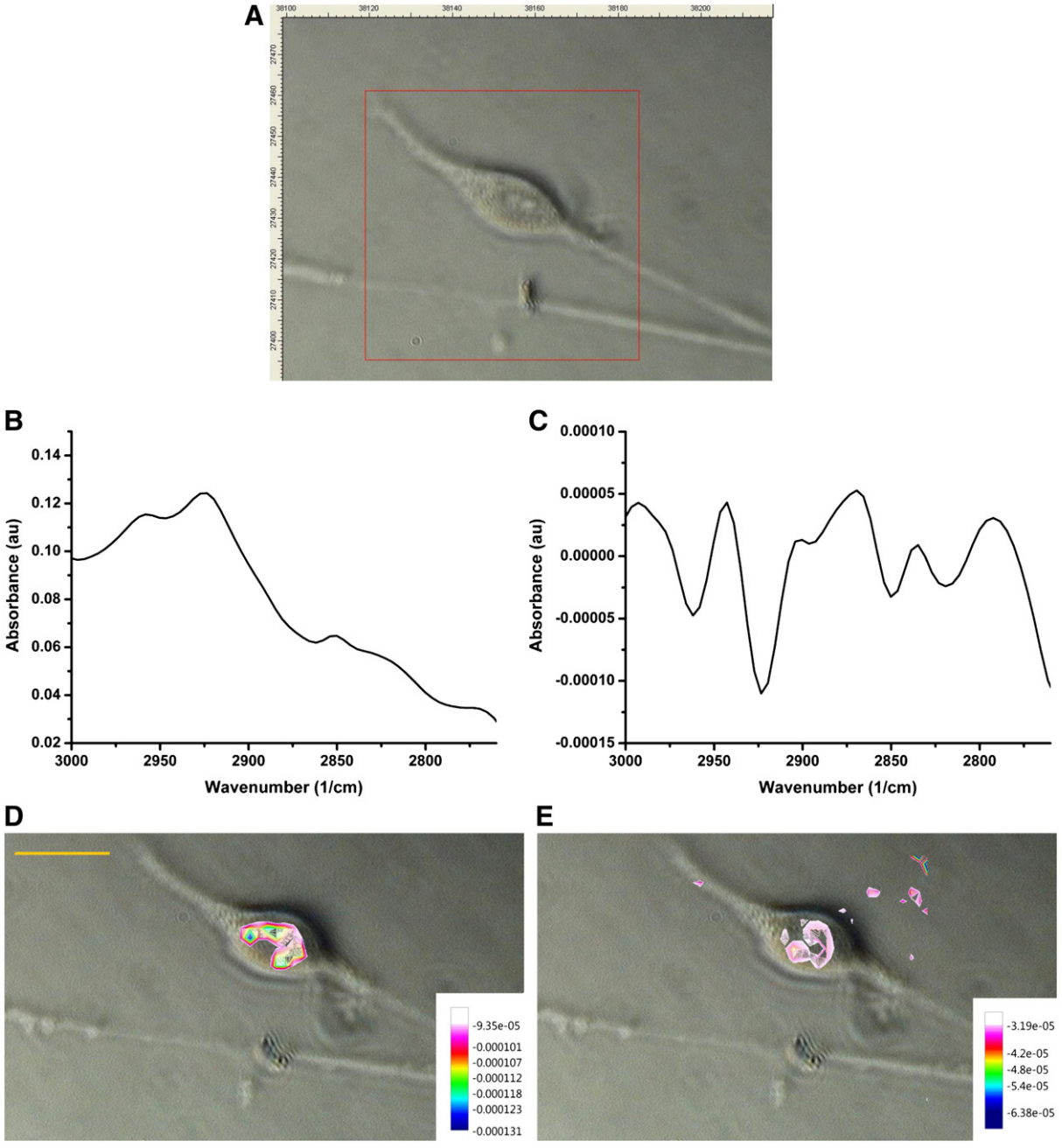

Fig. 1. Infrared absorption images of fibroblasts. The yellow bar corresponds to 20 μm. A — visible light image of a fibroblast cell. The scale on the surrounding frame is in micrometers. The red frame overlaid to the figure indicates the area probed by the FPA detector. B — absorption spectrum recorded from one cellular location. C — second derivative of the absorption spectrum. D — map of the distribution of second derivative intensity for the band at 2923 cm^{-1} E — map of the distribution of second derivative intensity for the band at 2965 cm^{-1}.

band at 2965 cm^{-1} are assigned to modes from methyl groups that cap the alkyl chains. This characteristic multiplet is a common feature in cellular samples due to the abundance of acylglycerolipids and sphingolipids [15]. Fig. 1C shows that the second derivative traces are of such quality that these spectral components can be resolved and mapped separately. The maps in Fig. 1D and E show the different distribution of two of these spectral components throughout the cell.

The difference in distribution shown in Fig. 1D and E can arise from a difference in the distribution of molecular components, from a difference in the organization of the acyl chains in membrane lipids, or from both. A difference in molecular composition is likely to be the dominant contribution. While the absorption band at 2923 cm^{-1} arises from acyl chain methylene groups, the band at 2965 cm^{-1} arises from methyl groups [15]. The former are mostly associated with acyl lipids in cellular membranes, which are the most abundant molecules that contain this group. The latter can be the same methyl groups that cap the acyl chains of lipids or methyl groups from other molecules present in the cell. In the IR absorption maps of several cell types, including fibroblasts, the location of the cell nucleus appears as a gap in the distribution of methylene groups due to the low density of acyl-rich membranes within the nucleus itself [16]. In contrast, the distribution of methyl groups is more uniform, reflecting the presence of an abundance and variety of methyl-containing molecules throughout the cell. In agreement with this interpretation, the distribution of methylene absorption in Fig. 1 shows a gap towards the middle of the cell, corresponding to the center of the putative nuclear location. Its maximal concentration is wrapped around the nuclear location, as expected from the distribution of the endoplasmic reticulum and the Golgi, which account for most of the cytoplasmic membranes. Also in agreement with this interpretation, the distribution of the methyl band appears more uniform and follows the topography of the cell.

It cannot be ruled out that the different distribution of the 2965 cm^{-1} and 2923 cm^{-1} bands contains a contribution from conformational differences in the acyl chains themselves. In preparations of ordered glycerolipids or lipid mixtures, such as supported phospholipid bilayers, both the ratio and peak position of the methylene and methyl bands are affected by molecular order within the membrane. Changes in the ordering of lipid chains induced by temperature, pressure, or membrane composition are reflected in changes of this ratio [17]. Nonetheless this contribution, if present, is expected to be minor in these maps, since in purified lipid preparations the relative change of this ratio due to phase transitions is of the order of a few percentage points.

3.2. Hydrogen/deuterium exchange kinetics

Exposure of the cells to a medium enriched in D_2O allows us to probe the kinetics of H/D exchange within the cell itself. Although exposure to large concentrations of D_2O is highly stressful, several cell types, including mammalian fibroblasts, can retain functionality for at least several hours [10,13].

Under these conditions, the different IR absorption properties of molecules containing ^1H or ^2H atoms can be used to obtain information about the structural and dynamic properties of specific biomolecules and of the cellular environment. Specifically, the use of different isotopes as tracers allows us to probe the flux of matter through the complex network of chemical reactions that comprise cellular biochemistry.

IR absorption measurements of fibroblasts exposed to a medium enriched in D_2O [10] show that the cells keep releasing measurable amounts of ^1H atoms in the water of the medium. It has been proposed that the ^1H atoms are transferred to the water pool from the metabolic turnover of ^1H-containing molecules [18,19]. A gradient of ^1H concentration between the interior and the exterior of the cell has been postulated, corresponding to a partial exclusion of D atoms from the interior of the cell. Despite the presence of this isotopic gradient, a partial isotopic shift of amide bands was observed, indicating that some deuteration still occurred in peptide groups. The experiments by Kreuzer et al. used wide confocal apertures and measured several cells and the intervening medium at the same time [10]. Therefore they could not confirm whether the observed deuteration of peptide bonds arises from cellular proteins, as opposed to proteins released in the extracellular medium. In the present work we now take advantage of the high spatial resolution and spectral quality of the measurement to analyze in detail the process of H/D exchange and verify that it is taking place within the cell, as opposed to in the extracellular medium.

The same set of measurements described in Fig. 1 was analyzed in the spectral region corresponding to the peptide bond absorption bands Amide I and Amide II, between 1700 and 1500 cm^{-1}. To report the localized evolution of the system, we averaged the spectra corresponding to selected subcellular locations, shown in Fig. 2B. Fig. 2C shows the time evolution of the averaged spectra. Spectral averaging allows us to improve the S/N ratio to a level that permits detection of small changes in the amide absorption bands. The trade-off is a loss in image oversampling, but it allows significant 2nd derivative analysis of the cell spectra. Spectra are measured at 20 minute time intervals over 200 min, and plotted as absorbance differences from the start of the measurement. Fig. 2D shows the expanded absorption of the Amide I and Amide II spectral region of the same spectra. Positive bands correspond to an increase in concentration while negative bands correspond to a decrease. A differential spectral pattern is clearly seen in the region of the Amide I peak, corresponding to a red shift of the position of Amide I. In addition, a decrease in absorbance is also observed around the region where the Amide II band is expected to fall, around 1550 cm^{-1}. The dominant spectral change is the large increase of absorbance observed around 1460 cm^{-1}.

The overall clarity of the band shifts is compromised by the baseline changes that accompany them. Baseline changes are often unavoidable in the spectra of functional cells since they can arise from a variety of morphological (e.g. cell shape or position) changes or chemical changes that affect its optical properties [2]. To simplify the analysis of the spectra and reduce the contribution of optical effects other than absorption, we report the second derivatives of the spectra in Fig. 2E. The second derivative of a Lorentzian/Gaussian band has a peak with opposite sign. Therefore an increase in the concentration of a species is seen a negative peak in Fig. 2E, while a decrease in the concentration is seen as a positive peak. Despite the decreased signal-to-noise ratio, the spectra in Fig. 2E clearly show the differential pattern due to the downshift of the Amide I peak. Deuteration of polypeptides is known to red shift the Amide I band by about 10 cm^{-1}, in agreement with Fig. 2E. Here the decrease of the Amide II band is also clearly detectable, despite the relative weakness of this band compared to Amide I. Due to the sharpness of the second derivative band profile, the strong absorption band increasing at ~1450 cm^{-1} is now revealed to be a composite peak, comprising at least a doublet at 1430 cm^{-1} and 1462 cm^{-1}.

Two main molecular species are expected to contribute to the latter multiplet. Previous work by Kreuzer et al. on cell clusters has already shown that a band increases at 1450 cm^{-1} following exposure of eukaryotic cells to large concentrations of D_2O. The band has been assigned to the bending mode of the isotopically mixed water molecule, δ_{HOD}, which is formed both intra- and extracellularly from the release of metabolically derived ^1H atoms [10]. In addition, H/D exchange of peptidic hydrogen is known to downshift the Amide II band of proteins by about 100 cm^{-1} to approximately 1450 cm^{-1} [15]. Indeed, a doublet at 1460 cm^{-1} and 1430 cm^{-1} has been reported for the Amide II of alpha-helical membrane proteins after H/D exchange [20]. The Amide II band of a protein after H/D exchange is commonly labeled as Amide II′, and we will use this notation throughout the text. A calculation of differences between the later spectra of Fig. 2E and F) shows that a weak doublet at 1430 cm^{-1} and 1463 cm^{-1} develops early during the measurement (during the first two acquired spectra) and stops growing soon afterwards. In contrast, a strong component that peaks at 1450 cm^{-1} keeps increasing over time throughout the measurement. The latter component dominates the apparent increase of

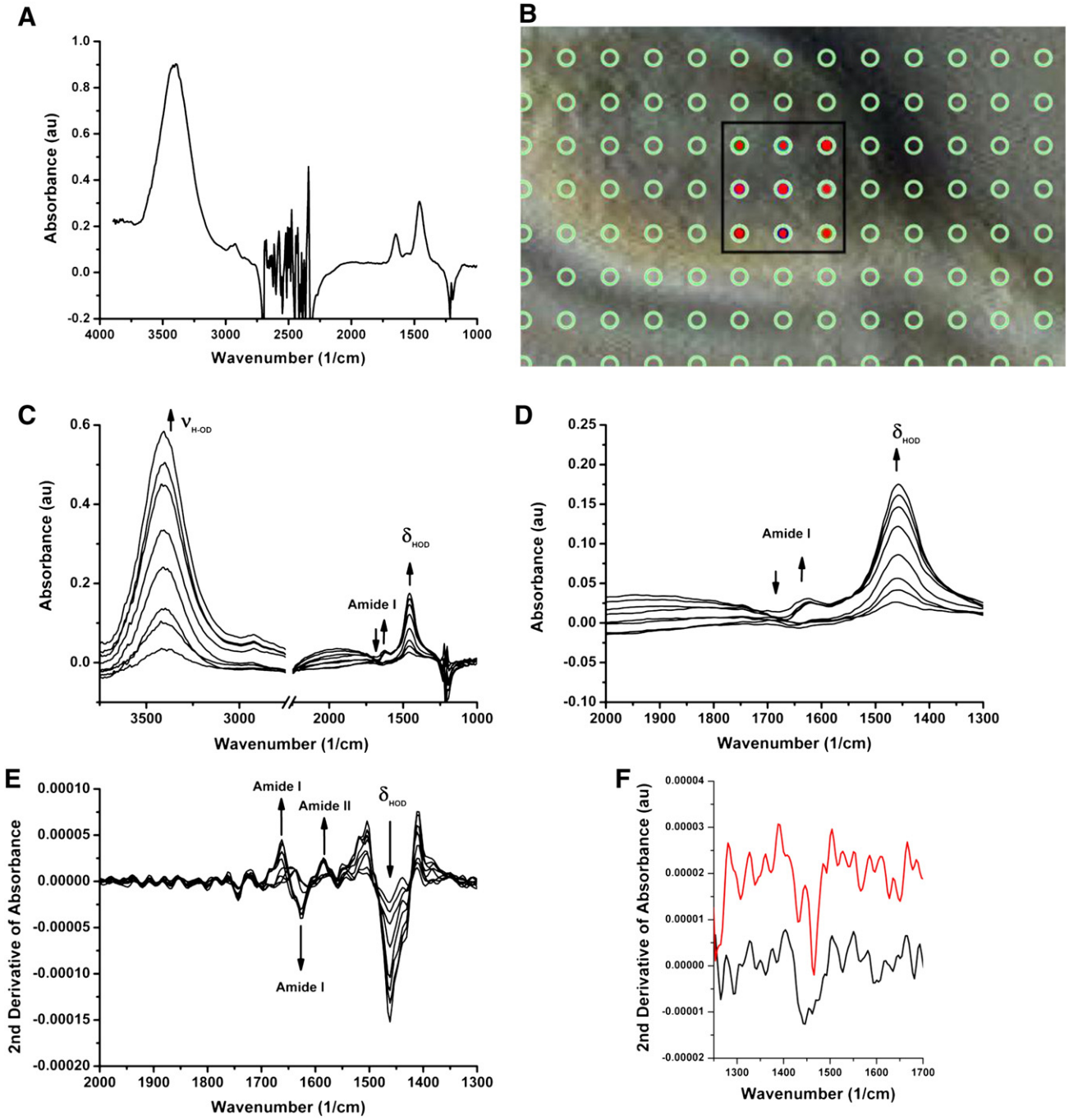

Fig. 2. Time resolved spectra recorded at 20 minute intervals from specific portions of the cell showing local H/D exchange patterns. A — extended absorption spectrum in the mid IR region from one pixel in the cellular region, recorded 200 min after exposure to D_2O. The spectrum is dominated by absorption from D_2O and HOD. The noisy range around 2500 cm^{-1} is caused by saturating absorption from D_2O. B — subcellular locations used for averaged spectral measurements. Each dot corresponds to the center of one pixel. The nine dark pixels enclosed in the frame are averaged to obtain one spectrum. C — averaged subcellular difference spectra plotted as a function of time. Spectra are plotted as absorbance differences from the start of the measurement. D — expansion of the 1300 cm^{-1}–2000 cm^{-1} region. E — second derivative of the spectra from panel C. F — subtractions between consecutive spectra of Fig. 2D, second derivative of absorbance; detail of the Amide II region. Top: second trace minus first trace. Bottom: eighth trace minus seventh trace.

intensity of the multiplet. We conclude that our IR measurements reveal both the presence of the Amide II′ mode of deuterated proteins and the accumulation of HOD molecules.

3.3. Isotopic gradients

The sensitivity of vibrational modes to isotopic substitutions offers the opportunity to study isotopic gradients in space by mapping the distribution of isotopically shifted bands throughout a sample. We performed this analysis on the cellular spectra used for Figs. 1 and 2. Fig. 3 displays the distribution of the second derivative of absorption at 1463 cm^{-1} and 1450 cm^{-1}, corresponding to a component of the Amide II′ band and to the δ_{HOD} band, respectively, in the surrounding of the fibroblast cell at different times after exposure to the D_2O enriched medium. Maps are shown at the start of the experiment, corresponding to t = 0, and afterwards at 100 and 200 min. The IR maps are plotted with a threshold excluding the lower absorbance range and plot only the regions with higher absorbance, to allow a clear overlay of molecular concentration profiles and the visible image of the cell. Different scales are used for the different panels of Fig. 3 and they

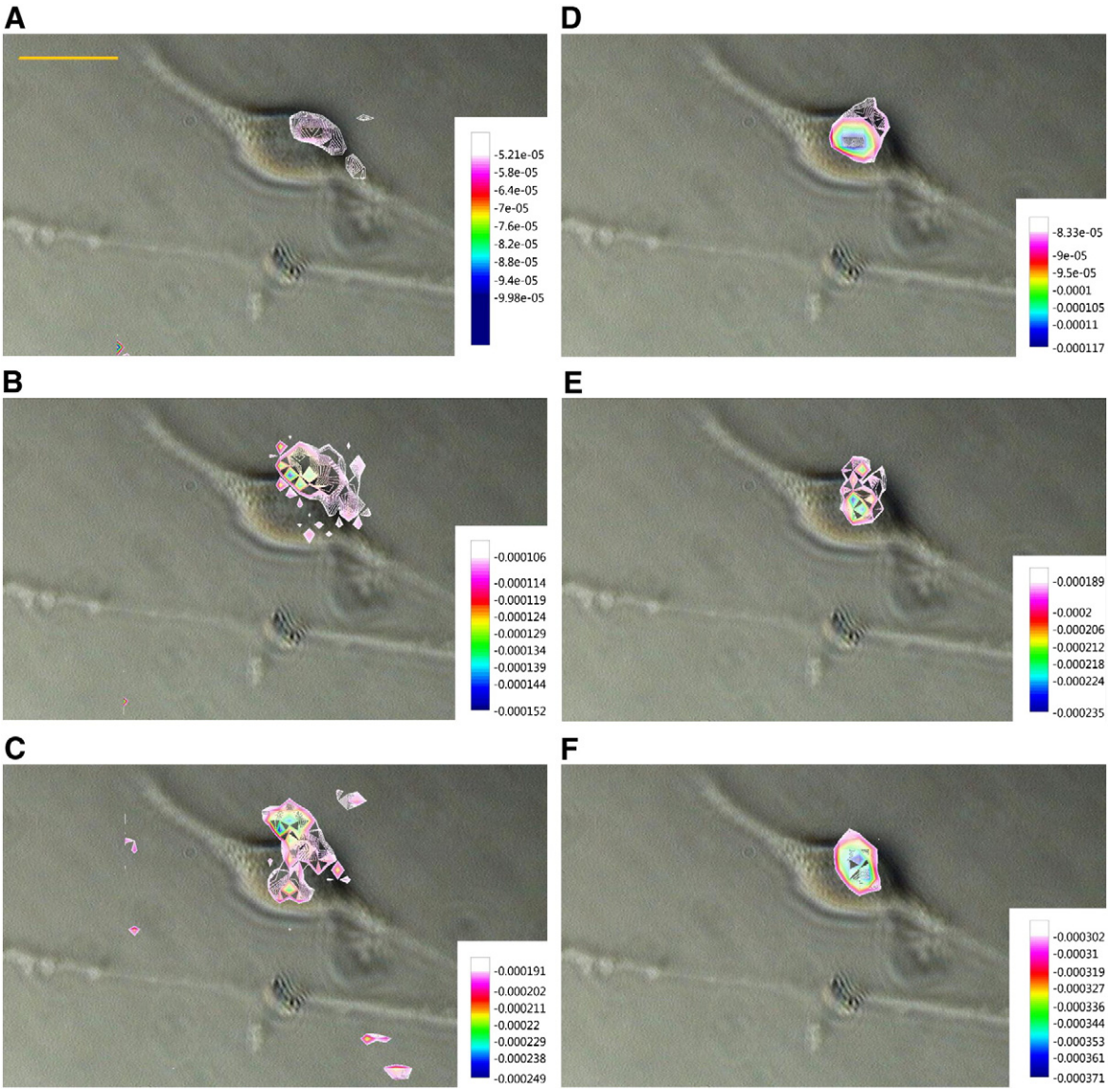

Fig. 3. Distribution of isotopically sensitive bands in the proximity of cells at t = 0, 100 and 200 min after the start of the measurement. The maps are built from plots of the 2nd derivative. The color-coded scale is in units of 2nd derivative of absorbance. The yellow bar corresponds to 20 μm. A, B, C — distribution of the δ_{HOD} band component at 1450 cm^{-1} at 0, 100 and 200 min respectively. D, E, F — distribution of the Amide II′ band component at 1463 cm^{-1} at 0, 100 and 200 min respectively. The color intensity scales are different for each figure and reported beside each of them.

reported beside the individual images. Absorbance at 1463 cm^{-1} and at 1450 cm^{-1} in both cases is localized in the proximity of the central part of the cell body. The Amide II′ band is clearly concentrated in the cell body (Fig. 3D, E, F), as expected from a band arising from cellular polypeptides. In contrast, the δ_{HOD} band is more diffuse (Fig. 3A, B, C), extending from the cell body towards the exterior of the cell on one side. The high degree of spectral overlap of the two bands prevents a complete separation of their spatial contributions. Nonetheless, spectra recorded away from the cytoplasm clearly indicate the absence of the Amide contribution in the medium. This observation demonstrates that the H/D exchange process affecting the Amide bands takes place in the cytoplasm of the cell and is *not* associated with proteins released outside of the cell. The band at 1450 cm^{-1} is weak at the start of the experiment and the color scale of the plot in Fig. 3A has been adjusted to highlight the very weak gradient. The gradient becomes steeper over time, but it appears to have reached a steady state by the end of the first hour (Fig. 3B). After this time the shape of the distribution of HOD still appears to fluctuate (not shown), presumably because of convection around the cell. In contrast, the distribution of the band at 1463 cm^{-1} remains localized on the cell body throughout the measurement, with only a small increase in total intensity, presumably due to the increase in the overlapping contribution from the δ_{HOD} band. The small spots observed away from the cell body in Fig. 3A to F correspond to residual contributions from noise and baseline effects that are not excluded by the offset correction.

The strong band due to the stretching mode of O – H in HOD, ν_{OH}, is expected to give plots similar to the ones of δ_{HOD}. However, the broadness of this band gives rise to second derivative peaks that are relatively weak compared to the background noise and therefore cannot be used to produce a map.

4. Discussion

To date, the vast majority of FTIR spectroscopy experiments have been performed on samples of purified biomolecules, at times reconstituted into structured assemblies such as membrane proteins in phospholipid bilayers, to simulate the complexity of their native environment [15,17,21,22]. Following successful application to simple biochemical systems,

interest has shifted towards spectroscopic measurements of more complex systems, i.e. cells and tissue [23,24]. In the early phases, activity was mostly driven by an interest in developing histopathology techniques based on vibrational spectroscopy [25,26]. As a result, most FTIR experiments on cells and tissue to date have been performed on preserved samples. However, in the pursuit of experimental techniques that allow detailed studies of biochemistry in vivo, the latest technical and methodological developments have addressed measurements in functional tissue and cells [2,27,28]. This later effort has resulted in several IR spectromicroscopy experiments showing the viability of dynamic measurements on single living cells and cell clusters [29].

The present work adds an important contribution to this body of work by showing the viability of spectromicroscopic IR measurements of processes within a single cell which extend both in time and in space. To maximize performance in terms of time and space resolution, the measurements take advantage of a bright synchrotron source coupled to a two-dimensional FPA detector for full-field IR microscopy.

The technical benefit of SR illumination versus globar illumination for full field IR imaging is still a consequence of the source brightness, as recently explained [30]. Specifically for the MIRIAM beamline optics, an ideal geometry using the 15× condenser for sample illumination and 36× objective for imaging (over a field of view area ~$70 \times 70\ \mu m^2$ corresponding to the 64×64 pixels FPA active chip) will result in at most a 20 times gain in flux per pixel under the IR microscope. The present experimental findings show an overall IR signal gain ranging from a factor 4 to 6 times per FPA pixel with IR sample illumination by a SR source versus a conventional one, which is consistent with the expectations.

It is worth noting that the detector 40 μm single pixel size is effectively 1.1 μm at the sample plane, while the best spatial resolution allowed by optical diffraction at the C–H band is 3 μm (equal to the wavelength, since the objective NA = 0.5). These conditions provide the image oversampling which, by Nyquist principle, must be a factor 2 times the scale of the minimum observable feature. In principle, further oversampling could be used to recover the ultimate diffraction limited spatial resolution λ/2 by deconvolving the instrument point spread function [30]. The practical approach we followed here is to exploit the synchrotron IR brightness to achieve high spectral quality at the single pixel level. Fig. 1B and C clearly shows that the signal-to-noise ratio achieved in this proof of principle experiment on a living cell is good enough to allow 2nd derivative analysis without noise enhancement, while Fig. 1D and E reveals that the IR map of the 2nd derivative signal is highly informative of the molecular structure at subcellular level. As calculated [6], there is an ideal pixel size that allows faithfully recording the entire absorption IR map without any loss of information, within the optical resolution limit of any imaging system. In the mid-IR wavenumber range a 4000 cm^{-1} the equivalent pixel size at the sample for an objective with NA = 0.5 has to be ideally 1.25 μm. This value is consistent with the pixel size in our experiments, and more generally the theoretical calculation provides the background model supporting the use of the current set up for full field IR microscopy via SR at MIRIAM beamline.

An additional complication that can be addressed is the presence of an aqueous sample environment. This is challenging for IR spectroscopy, because of the strong absorption from water that causes a significant throughput reduction. Synchrotron illumination gives a clear advantage in terms of increased photon flux density relative to the globar, which allows enough signal at single pixel level for proper absorption calculation.

We show that classical FTIR experiments, extensively performed on purified molecules and simple mixtures, are viable in single cells with resolution down to the subcellular level. We now discuss some of the main possibilities.

4.1. Spatial and spectral resolution of bands from C–H stretching vibrations

Accurate measurements of the relative intensity and position of bands from C–H stretching modes have been used extensively to probe the structure of biological membranes and their lipid constituents. In particular, the position of the symmetric and antisymmetric CH_2 stretching bands ($\nu_{s,\ CH2}$ and $\nu_{as,\ CH2}$, respectively) is a sensitive indicator of phase transitions in lipid membranes [17]. The ratio between the bands of CH_2 and CH_3 stretching modes is also sensitive to the conformation of long acyl chains. In anisotropic systems, the orientation of the membrane and the functional groups of its constituents can also be assessed quantitatively by using these bands. Much past research on the phase diagram of membranes and their models has been based on the use of these peaks. Being able to perform such measurements in a living cell is a valuable tool for the study of biochemistry in vivo. To date only one detailed FTIR study of membrane properties in an intact cell has been reported [31]. This work was based on spectromicroscopy measurements on the outer segment of a retinal rod cell (ROS) and took advantage of the sharp separation of this cellular compartment from the cell body to probe selectively ROS membranes. Unfortunately the structure of a ROS is fairly unique and dictated by its highly specialized function as a photoreceptor. Most membrane structures in cells have a complex spatial distribution and their absorption bands overlap with the bands of other molecular components containing C–H bonds. Resolving, at least partially, this complexity requires high spectral resolution in measurements performed with high spatial resolution. Our results show the possibility of achieving both while measuring a functional cell. The quality of the spectral measurements is such as to allow spatial discrimination of CH_2 and CH_3 components with spatial resolution close to the diffraction limit. This is the first time that this level of resolution is reported for living cells. The latter feature is critical for the accurate characterization of cellular membranes, the structure of which is disrupted when the cells are dried.

4.2. Measurement of H/D exchange in cellular polypeptides

H/D exchange has been used extensively in studies of biomolecules as a tool to extract both structural and dynamic information [21]. The rate of replacement of exchangeable H atoms with D atoms in proteins is a tool to assess the solvent accessibility of residues and main chain peptide bonds in proteins [32]. In some cases, the functional role of specific H atoms could also be probed by measuring their rate of exchange. In more complex systems, the interaction between intrinsic proteins and their host membranes could be evaluated [15]. These experiments provided valuable structural information on proteins at a time when the number of x-ray diffraction and NMR structures available was limited. With the current increase in the throughput of macromolecular structures, including the most challenging membrane proteins, measurements of H/D exchange have lost much of their value in the study of pure biomolecules. However, our present results show that this type of experiment is also feasible for polypeptides in living cells. Inside a cell, biological macromolecules are in their native environment, constrained in their mobility, in the presence of all their interacting molecular partners, and exposed to an aqueous environment which is very different from that of a classical solution. Under these conditions, the structural properties that affect H/D exchange processes may be very different from those recorded in solutions of the pure molecule. Novel insight into macromolecular structure and function could become available that is specific to the cellular environment. The complexity of a cell is of course much greater than that of a single protein in solution and interpreting H/D exchange data in vivo will be a major challenge. Nonetheless, the dearth of molecular information on cellular structures in vivo makes this type of study a plausible tool. The use of a sequential imaging format for the measurement delivers structural and dynamic information with a single experiment. Furthermore, the use of an imaging approach allows us the added benefit of coupling H/D exchange measurements in specific cellular locations to the measurement of isotopic flux between cellular compartments and between cells, as detailed in the next paragraph.

4.3. Spatial visualization of isotopic gradients

Using isotope ratio mass spectrometry (IRMS) and FTIR spectromicroscopy, Kreuzer et al. demonstrated that metabolic fluxes of O and H can be detected in laboratory cultures of prokaryotic and eukaryotic cells and in animal tissue [10,18,19]. In particular, eukaryotic cells exposed to medium with a high concentration of D_2O kept releasing ^1H atoms into the cytoplasm and extracellular medium [10]. It is postulated that the ^1H atoms originate from the atoms of nutrients in the medium, which are introduced into the water pool by a variety of metabolic processes. IRMS work led to the proposal that this flow is associated with the formation of an isotopic gradient between the extracellular and intracellular spaces. Fig. 3 provides the first visual representation of such a gradient, opening the way for its quantitative characterization and manipulation, as well as the study of its physiological implications. It is important to note that the gradient can be appreciated only in the proximity of the cell. Large concentrations of HOD molecules are present throughout the medium, but their concentration is practically constant some 20 μm away from the cell. The diffusion of $^1H^+$ atoms through D_2O is characterized by a coefficient of 500 $\mu m^2/s$. Rapid diffusion accounts for the rapid plateauing of the HOD concentration away from the cell membrane. The constant contribution from HOD absorption away from the cell is not shown in Fig. 3. For clarity the limits of the intensity scale have been selected to remove it from the plot and highlight only the region where the gradient is visible.

It is interesting to note that the gradient is not symmetrically distributed around the cell. Instead, it develops slowly on one side but is steeper on the opposite side. This asymmetry is maintained throughout the measurement, as the gradient develops from Fig. 3A to C. This observation is reproducible. One possible explanation of its origin is that a larger accumulation of ^1H atoms is present on one side of the cell because of the specific cellular localization of transporter and pore proteins responsible for water and H^+ exchange. The steepness of the gradient is expected to depend on the rate of H atom transfer across the cellular membrane relative to the rate of H atom diffusion through the medium. However, sufficient evidence to support a specific interpretation is lacking at the present time. Additional systematic experiments are under way to clarify the occurrence and the origin of this feature.

Measurement of the gradient is a step forward towards the quantitative assessment of cellular H/D exchange rates, as discussed in the previous section, since the local value of the concentration of D_2O or HOD in the cell affects the rate of H/D exchange for macromolecules in that location. It also creates an opportunity to study a variety of other cellular processes by using substrates with appropriate isotopic labels. Possible examples include the kinetics of membrane translocation of hydrogen and oxygen, the rate of metabolic substrate turnover, and the flow of metabolites through different pathways.

5. Conclusions

Here we demonstrate that the use of synchrotron infrared imaging with an FPA detector allows visualization and quantification of specific cellular properties with both spatial and temporal resolution. The method opens the way to performing classical experiments of biochemical spectroscopy on living cells. We consider three specific types of experiments. The first two have been extensively applied to the study of purified biological molecules and have become workhorses of biochemical spectroscopy. In the first case we show that structurally-relevant properties of lipid membranes can be described in vivo, together with their distribution. In the second case we demonstrate the viability of H/D exchange measurements in specific cellular locations. In the third type of experiment, we show the quantitative assessment of isotopic H and O concentration gradients in the proximity of an actively metabolizing cell. The measurements can be performed with spatial resolution at the subcellular level. Dynamic processes can be studied with a time resolution on the order of a minute. In parallel, spectroscopic information can be easily obtained with a spectral resolution of 4 cm^{-1}, sufficient for most vibrational spectroscopy experiments on biological systems.

Additional experiments can also be designed based on this general procedure, taking advantage of the multiplexing capabilities of FTIR spectroscopy, which allow simultaneous detection of the whole mid IR spectral range. Detection and imaging in real time of metabolite distributions [5], major protein conformational changes [33], lipid oxidation [34], phosphorylation [35], and cellular hydration and acidity [36] are all applications that can all be envisioned based on the performance demonstrated in this work, opening the way to a detailed description of cellular biochemistry and biophysics in real time.

Acknowledgement

LQ acknowledges the support for research expenses from the internal funding of the Paul Scherrer Institut. The research leading to these results has received funding from the European Community's Seventh Framework Programme (FP7/2007-2013) under grant agreement nº 226716 via proposal SM5773 for beamtime allocated at the MIRIAM beamline of Diamond Light Source within the CALIPSO program.

References

[1] I.W. Levin, R. Bhargava, Fourier transform infrared vibrational spectroscopic imaging: integrating microscopy and molecular recognition, Annu. Rev. Phys. Chem. 56 (2005) 429–474.
[2] L. Quaroni, T. Zlateva, Infrared spectromicroscopy of biochemistry in functional single cells, Analyst 136 (2011) 3219–3232.
[3] H.-Y.N. Holman, H.A. Bechtel, Z. Hao, M.C. Martin, Synchrotron IR spectromicroscopy: chemistry of living cells, Anal. Chem. 82 (2011) 8757–8765.
[4] S.G. Kazarian, K.L.A. Chan, ATR-FTIR spectroscopic imaging: recent advances and applications to biological systems, Analyst 138 (2013) 1940–1951.
[5] K.L. Goff, L. Quaroni, K.E. Wilson, Measurement of metabolite formation in single living cells of *Chlamydomonas reinhardtii* using synchrotron Fourier-transform Infrared spectromicroscopy, Analyst 134 (2009) 2216–2219.
[6] R.K. Reddy, M.J. Walsh, M.V. Schulmerich, P.S. Carney, R. Bhargava, High-definition infrared spectroscopic imaging, Appl. Spectrosc. 67 (2013) 93–105.
[7] M.J. Nasse, M.J. Walsh, E.C. Mattson, R. Reininger, A. Kajdacsy-Balla, V. Macias, R. Bhargava, C.J. Hirschmugl, High-resolution Fourier-transform infrared chemical imaging with multiple synchrotron beams, Nat. Methods 8 (2011) 413–416.
[8] G.L. Carr, L.M. Miller, P. Dumas, Synchrotron radiation as a Source for infrared microspectroscopy imaging with 2D multi-element detection, in: D. Moss (Ed.), Biomedical Applications of Synchrotron Infrared Spectromicroscopy, Royal Society of Chemistry, Cambridge, 2011, pp. 226–259.
[9] C. Petibois, G. Deleris, M. Piccinini, M. Cestelli-Guidi, A. Marcelli, A bright future for synchrotron imaging, Nat. Photonics 3 (2009) 179.
[10] H.W. Kreuzer, L. Quaroni, D.W. Podlesak, T. Zlateva, N. Bollinger, A. McAllister, M.J. Lott, E.L. Hegg, Detection of metabolic fluxes of O and H atoms into intracellular water in mammalian cells, Public Libr. Sci. ONE 7 (2012) e39685.
[11] G. Cinque, M. Frogley, K. Wehbe, J. Filik, J. Pijanka, Multimode infrared imaging and microspectroscopy (MIRIAM) beamline at Diamond, Synchrotron Radiat. News 24 (2011) 24–33.
[12] G. Cinque, M. Frogley, Multiple element infrared synchrotron mirrors, AIP Conf. Proc. 1214 (2010) 29–31.
[13] D.J. Kushner, A. Baker, T.G. Dunstall, Pharmacological uses and perspectives of heavy water and deuterated compounds, Can. J. Physiol. Pharmacol. 77 (1999) 79–88.
[14] R. Zhao, L. Quaroni, A.G. Casson, Fourier transform infrared (FTIR) spectromicroscopic characterization of stem-like cell populations in human esophageal normal and adenocarcinoma cell lines, Analyst 135 (2010) 53–61.
[15] L.K. Tamm, S.A. Tatulian, Infrared spectroscopy of proteins and peptides in lipid bilayers, Q. Rev. Biophys. 30 (1997) 365–429.
[16] P. Lasch, A. Pacifico, M. Diem, Spatially resolved IR microspectroscopy of single cells, Biopolymers 61 (2002) 335–338.
[17] R.N.A.H. Lewis, R.N. McElhaney, Membrane lipid phase transitions and phase organization studied by Fourier transform infrared spectroscopy, Biochim. Biophys. Acta Biomembr. 1828 (2013) 2347–2358.
[18] H.W. Kreuzer-Martin, J.R. Ehleringer, E.L. Hegg, Oxygen isotopes indicate most intracellular water in log-phase *Escherichia coli* is derived from metabolism, Proc. Natl. Acad. Sci. U. S. A. 102 (2005) 17337–17341.
[19] H.W. Kreuzer-Martin, M.J. Lott, J.R. Ehleringer, E.L. Hegg, Metabolic processes account for the majority of the intracellular water in log-phase *Escherichia coli* cells as revealed by hydrogen isotopes, Biochemistry 45 (2006) 13622–13630.
[20] J. le Coutre, H.R. Kaback, C.K.N. Patel, L. Heginbotham, C. Miller, Fourier transform infrared spectroscopy reveals a rigid alpha-helical assembly for the tetrameric *Streptomyces lividans* K + channel, Proc. Natl. Acad. Sci. U. S. A. 95 (1998) 6114–6117.
[21] J.L.R. Arrondo, F.M. Goni, Structure and dynamics of membrane proteins as studied by infrared spectroscopy, Prog. Biophys. Mol. Biol. 72 (1999) 367–405.

[22] Z. Arsov, L. Quaroni, Detection of lipid phase coexistence and lipid interactions in sphingomyelin/cholesterol membranes by ATR-FTIR spectroscopy, Biochim. Biophys. Acta Biomembr. 1778 (2008) 880–889.
[23] M. Diem, M.J. Romeo, S. Boydston-White, C. Matthaus, IR Spectroscopic Imaging. From Cells to Tissue, Spectrochemical Analysis Using Infrared Multichannel Detectors, 2005. 189–203.
[24] C. Matthaus, B. Bird, M. Miljkovic, T. Chernenko, M. Romeo, M. Diem, Infrared and Raman microscopy in cell biology, Biophysical Tools for Biologists, Vol 2, in Vivo Techniques, 892008. 275–308.
[25] M. Diem, P.R. Griffiths, J.M. Chalmers (Eds.), Vibrational Spectroscopy for Medical Diagnosis, 2008.
[26] P. Lasch, L. Chiriboga, H. Yee, M. Diem, Infrared spectroscopy of human cells and tissue: detection of disease, Technol. Cancer Res. Treat. 1 (2002) 1–7.
[27] J.R. Mourant, Y.R. Yamada, S. Carpenter, L.R. Dominique, J.P. Freyer, FTIR spectroscopy demonstrates biochemical differences in mammalian cell cultures at different growth stages, Biophys. J. 85 (2003) 1938–1947.
[28] E.J. Marcsisin, C.M. Uttero, M. Miljkovic, M. Diem, Infrared microspectroscopy of live cells in aqueous media, Analyst 135 (2010) 3227–3232.
[29] L. Quaroni, T. Zlateva, E. Normand, Detection of weak absorption changes from molecular events in time-resolved FT-IR spectromicroscopy measurements of single functional cells, Anal. Chem. 83 (2011) 7371–7380.
[30] E. Stavitski, R.J. Smith, M.W. Bourassa, A.S. Acerbo, G.L. Carr, L.M. Miller, Dynamic full-field infrared imaging with multiple synchrotron beams, Anal. Chem. 85 (2013) 3599–3605.
[31] L. Quaroni, T. Zlateva, D. Bedolla, S. Massaro, V. Torre, Measurement of molecular orientation in a subcellular compartment by synchrotron infrared spectromicroscopy, ChemPhysChem 9 (2008) 1380–1382.
[32] J.S. Vrettos, C.W. Meuse, Infrared techniques for quantifying protein structural stability, Anal. Biochem. 390 (2009) 14–20.
[33] M. Bonda, V. Perrin, B. Vileno, H. Runne, A. Kretlow, L. Forro, R. Luthi-Carter, L.M. Miller, S. Jeney, Synchrotron infrared microspectroscopy detecting the evolution of Huntington's disease neuropathology and suggesting unique correlates of dysfunction in white versus gray brain matter, Anal. Chem. 83 (2011) 7712–7720.
[34] B. Vileno, S. Jeney, A. Sienkiewicz, P.R. Marcoux, L.M. Miller, L. Forro, Evidence of lipid peroxidation and protein phosphorylation in cells upon oxidative stress photo-generated by fullerols, Biophys. Chem. 152 (2010) 164–169.
[35] L. Chen, H.-Y.N. Holman, Z. Hao, H.A. Bechtel, M.C. Martin, C. Wu, S. Chu, Synchrotron infrared measurements of protein phosphorylation in living single PC12 cells during neuronal differentiation, Anal. Chem. 84 (2012) 4118–4125.
[36] M. Carbone, T. Zlateva, L. Quaroni, Monitoring and manipulation of the pH of single cells using infrared spectromicroscopy and a molecular switch, Biochim. Biophys. Acta Gen. Subj. 1830 (2013) 2989–2993